ELSEVIER

Physica D 82 (1995) 165–179

PHYSICA D

Unstable wavetrains and chaotic wakes in reaction-diffusion systems of λ–ω type

Jonathan A. Sherratt [1]

Nonlinear Systems Laboratory, Mathematics Institute, University of Warwick, Coventry CV4 7AL, UK

Received 5 August 1994; revised 14 November 1994; accepted 16 November 1994
Communicated by A.V. Holden

Abstract

Periodic wavetrains are the one-dimensional equivalent of spiral waves and target patterns, and play a crucial role in the dynamics of oscillatory reaction-diffusion equations. I consider the behaviour of a λ–ω system of reaction-diffusion equations on a one-dimensional finite spatial domain with boundary conditions corresponding to the forcing of a particular periodic wavetrain. I derive a condition for the wavetrain itself to be a stable solution, and present numerical evidence for a complex sequence of bifurcations in the unstable region of parameter space. Finally I discuss the implications of the results for the phenomenon of irregular wakes behind transition waves in reaction-diffusion equations.

1. Introduction

Periodic wavetrains are waves moving with constant shape and speed that oscillate in both space and time. In systems of reaction-diffusion equations whose kinetics have a stable limit cycle, periodic wavetrains, also known as periodic plane waves, are a vitally important type of solution. Spiral waves and target patterns, which have been intensively studied as solutions of oscillatory reaction-diffusion equations [e.g. 1,2], both approach periodic plane waves at large distances from their centres. Moreover in one space dimension, many initial conditions relevant in applications evolve to periodic wavetrains [3,4].

Since they were first studied by Kopell and Howard more than twenty years ago [9], much of the understanding of periodic plane waves has been gained from λ–ω systems. This is a simple class of oscillatory reaction-diffusion equations, with the form

$$u_t = u_{xx} + \lambda(r)u - \omega(r)v, \tag{1a}$$

$$v_t = v_{xx} + \omega(r)u + \lambda(r)v. \tag{1b}$$

[1] E-mail: jas@maths.warwick.ac.uk

SSDI 0167-2789(94)00224-X

Here $r = (u^2+v^2)^{1/2}$, u and v are functions of space x and time t, subscripts x and t denote partial derivatives, and $\lambda(0)$ and $\omega(0)$ are strictly positive. For simplicity I take $\lambda(r)$ to be monotonically decreasing with a zero at $r = r_L$, so that the kinetics have a stable, circular limit cycle with radius r_L. In this case, there is a one parameter family of periodic plane waves, given by

$$u = r_0 \cos\left[\omega(r_0)t \pm \lambda(r_0)^{1/2}x\right], \tag{2a}$$

$$v = r_0 \sin\left[\omega(r_0)t \pm \lambda(r_0)^{1/2}x\right], \tag{2b}$$

with $0 < r_0 < r_L$. It is most convenient to work with polar coordinates in u–v space, that is $r = (u^2+v^2)^{1/2}$, $\theta = \tan^{-1}(v/u)$. In terms of these variables, the periodic plane wave solutions are $r = r_0$, constant, with θ a linear function of space and time. It is because of this simplicity of representation that λ–ω systems are often used as a prototype for more general oscillatory reaction-diffusion equations.

A key issue is whether periodic plane waves are stable as solutions of the partial differential equations. Despite intensive study [5–8] the full answer to this in general reaction-diffusion equations remains unclear. However for λ–ω systems, it was shown in the original paper of Kopell and Howard [9] that the periodic plane wave solution (2) is stable as a solution of (1) on an infinite spatial domain if and only if r_0 satisfies

$$4\lambda(r_0)\left[1+\left(\frac{\omega'(r_0)}{\lambda'(r_0)}\right)^2\right] + r_0\lambda'(r_0) \leq 0. \tag{3}$$

The aim of this paper is to consider the way in which the solution of (1) evolves from a periodic wavetrain when a parameter is altered so that the wavetrain becomes unstable. In order to give a closer connection with applications, as well as to enable numerical study, I consider a finite spatial domain, and thus I start by considering the equivalent of the stability condition (3) in a finite domain. I will then describe the solutions when this stability condition is not satisfied. My results have important implications for the phenomenon of irregular wakes behind invasive transition waves that I have described previously [3], and I will discuss this in Section 4.

2. Stability of periodic plane waves on a finite domain

Periodic plane wave solutions only exist on a finite domain if suitable boundary conditions are applied. One obvious possibility for such boundary conditions is periodicity in u, v and their first derivatives; however, in this case a particular periodic plane wave solution only exists for certain discrete values of the domain length, which prevents the use of the domain length as a continuous bifurcation parameter. To overcome this difficulty, I consider instead imposing the values of r_x and θ_x on the boundary. Specifically, I consider the system (1) on $0 < x < L$, subject to

$$r_x = 0, \quad \theta_x = \sqrt{\lambda(r_0)} \quad \text{or equivalently } u_x = -v\sqrt{\lambda(r_0)}, \quad v_x = +u\sqrt{\lambda(r_0)} \tag{4}$$

at $x = 0$ and $x = L$. At first sight these boundary conditions may appear rather artificial. However, they correspond to periodic plane waves being forced at the boundary of the domain, and this situation does in fact arise in the specific case of irregular wakes behind invasive wave fronts; I will describe this in detail in Section 4.

When expressed in terms of the polar coordinates r and θ, (1) is

$$r_t = r\lambda(r) + r_{xx} - r\theta_x^2, \tag{5a}$$

$$\theta_t = \omega(r) + \theta_{xx} + 2r_x\theta_x/r. \tag{5b}$$

Linearising about the periodic plane wave solution $r = r_0$, $\theta = \lambda(r_0)^{1/2}x + \omega(r_0)t$ gives

$$\rho'' + 2\lambda(r_0)^{1/2}r_0\phi' + [r_0\lambda'(r_0) - \nu]\rho = 0, \tag{6a}$$

$$\phi'' - 2\rho'\lambda(r_0)^{1/2}/r_0 - \nu\phi + \omega'(r_0)\rho = 0, \tag{6b}$$

subject to

$$\rho' = \phi' = 0 \quad \text{at } x = 0 \text{ and } x = L. \tag{7}$$

Here prime denotes d/dx and $r(x,t) = r_0 + \rho(x)\exp(\nu t)$, $\theta(x,t) = \lambda(r_0)^{1/2}x + \omega(r_0)t + \phi(x)\exp(\nu t)$; without loss of generality I am considering only periodic plane waves moving in the negative x direction. The periodic plane wave is linearly stable if and only if there are no non-trivial solutions of (6) and (7) with $\mathrm{Re}(\nu) > 0$. Note that ν, ρ and ϕ are in general all complex valued.

The system (6) is a fourth order set of ordinary differential equations in which the domain length L and the amplitude r_0 of the periodic wavetrain are parameters. The system is most conveniently rewritten in the form $\underline{Y}' = \underline{\underline{A}}\,\underline{Y}$, where $\underline{Y} = (\rho, \rho', \phi, \phi')$. Straightforward calculation shows that the eigenvalues $\lambda_1, \ldots, \lambda_4$ of this system at $(0,0,0,0)$ are the roots of

$$\lambda^4 + [4\lambda(r_0) + r_0\lambda'(r_0) - 2\nu]\lambda^2 - 2\lambda(r_0)^{1/2}r_0\omega'(r_0)\lambda + [\nu^2 - \nu r_0\lambda'(r_0)] = 0. \tag{8}$$

Denoting by $\underline{v}_i$ the eigenvector corresponding to λ_i, the general solution of (6) is then

$$\underline{Y}(x) = \sum_{i=1}^{4} k_i\underline{v}_i\exp(\lambda_i x),$$

where $k_1, \ldots, k_4$ are constants of integration. The boundary conditions impose conditions on the k_is:

$$\sum_{i=1}^{4} k_i(\underline{v}_i)_2 = \sum_{i=1}^{4} k_i(\underline{v}_i)_4 = \sum_{i=1}^{4} k_i(\underline{v}_i)_2\exp(\lambda_i L) = \sum_{i=1}^{4} k_i(\underline{v}_i)_4\exp(\lambda_i L) = 0,$$

where $(\underline{v}_i)_j$ denotes the jth component of the ith eigenvector. Therefore there is a non-trivial solution of (6) subject to (7) if and only if

$$D \equiv \det\begin{bmatrix} (\underline{v}_1)_2 & (\underline{v}_1)_4 & (\underline{v}_1)_2\exp(\lambda_1 L) & (\underline{v}_1)_4\exp(\lambda_1 L) \\ (\underline{v}_2)_2 & (\underline{v}_2)_4 & (\underline{v}_2)_2\exp(\lambda_2 L) & (\underline{v}_2)_4\exp(\lambda_2 L) \\ (\underline{v}_3)_2 & (\underline{v}_3)_4 & (\underline{v}_3)_2\exp(\lambda_3 L) & (\underline{v}_3)_4\exp(\lambda_3 L) \\ (\underline{v}_4)_2 & (\underline{v}_4)_4 & (\underline{v}_4)_2\exp(\lambda_4 L) & (\underline{v}_4)_4\exp(\lambda_4 L) \end{bmatrix} = 0. \tag{9}$$

This is the dispersion relation, determining the eigenvalues ν for which (6) subject to (7) has a non-trivial solution. Since both the real and imaginary parts of the determinant must be zero, there are two scalar equations, which determine both the real and imaginary parts of ν.

It is algebraically unfeasible to solve (8) analytically for the eigenvalues λ_i; however, numerical solution is straightforward. To this end I introduce at this stage the following specific forms for $\lambda(.)$ and $\omega(.)$:

$$\lambda(r) = 1 - r^2, \quad \omega(r) = 3 - r^2. \tag{10}$$

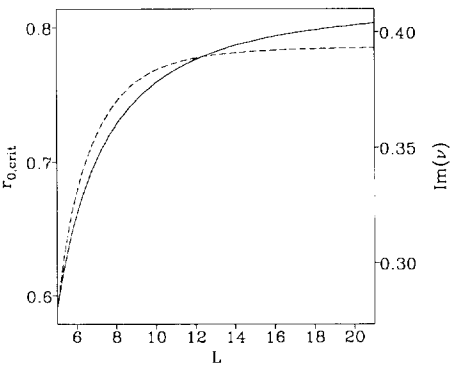

Fig. 1. The variation of $r_{0,crit}$ with the domain length L (————). The periodic wavetrain with amplitude r_0 is stable as a solution of (1) subject to (4) if and only if $r_0 > r_{0,crit}$. I also show the corresponding variation in Im(ν) (- - - - - - - - -), which is the temporal frequency of the neutrally stable perturbations at $r_0 = r_{0,crit}$.

All numerical results presented in this paper use these particular functional forms (except that in Section 4 a slight variant is also used); their choice is essentially arbitrary. However, less extensive numerical solutions with a range of other functional forms suggest that in all cases qualitatively similar behaviour occurs more generally.

Having specified particular functions, it is straightforward to calculate λ_i, $\underline{v}_i$ and thence D numerically for any given values of L and r_0, which are the only remaining parameters. However, numerical calculation of the zeros of D has a slight difficulty. The reason is that the sign of D depends on the ordering of the λ_is, which cannot be regulated in numerical solution. Therefore sudden changes in the sign of the calculated value of D can occur, and the difficulty is to distinguish these from zeros. I found that elimination of these spurious zeros required careful comparison of the changes in the actual and absolute values of the real and imaginary parts of D.

For the functional forms (10), the stability condition (3) for an infinite domain is simply $r_0 > 2/\sqrt{5} \approx 0.89$ for stability. Intuitively, one expects that on a finite domain, the corresponding condition will be $r_0 > r_{0,crit}(L)$, where $r_{0,crit}$ is a critical value that increases with L. In order to determine this anticipated critical value numerically, I focus only on changes of stability, and impose $\mathrm{Re}(\nu) = 0$. The real and imaginary parts of D are then functions of r_0, $\mathrm{Im}(\nu)$ and L, and changes in stability occur at values of these three quantities at which both the real and imaginary parts of D are zero. The critical value $r_{0,crit}(L)$ is simply the largest value of r_0 at which $\mathrm{Re}(D)$ and $\mathrm{Im}(D)$ have a common zero; the corresponding value of $\mathrm{Im}(\nu)$ is the temporal frequency at which the neutrally stable perturbations oscillate. Fig. 1 shows the variation of $r_{0,crit}$ with L, calculated in the way I have described; the corresponding values of $\mathrm{Im}(\nu)$ are also shown. Extensive numerical solutions confirm that for a given domain length L, periodic plane wave solutions are indeed stable to small perturbations below this critical amplitude and unstable above it.

3. Behaviour in the unstable region

Having discussed the conditions for the periodic plane wave solution of (5) subject to (4) to be linearly stable, I now consider the behaviour of the equations in the unstable region of parameter space. The work in this section is entirely numerical, and all my results will be for the particular kinetics given by (10). Therefore there are only two parameters in the problem: the domain length L and the periodic plane wave amplitude r_0 induced on the boundary. However the range of behaviour in the unstable region $r_0 < r_{0,crit}(L)$ is in fact

very rich, and it is computationally unfeasible to attempt a detailed study of the entire r_0–L parameter space. Therefore I restrict attention to the behaviour as r_0 is varied with $L = 5$ and $L = 30$. These domain sizes should be considered in relation to the spatial wavelength of the periodic waves, which varies between 6.3 and 13.8 for stable wave numbers. For these domain lengths I will describe the way in which the long term behaviour of the solutions changes with the parameter r_0. This approach is reminiscent of that used by Moon et al. [10] and others [11,12] to study bifurcations in the Ginzburg–Landau equation as the domain length varies. These studies have shown transitions to chaos via two- and three-tori as the domain length increases with periodic, Neumann and Dirichlet boundary conditions. There are two key differences between this previous work and the present study. The first is that a particular solution is not forced on the boundary, in contrast to the boundary condition (4) which is central to the results I will discuss. The second is that the Ginzburg–Landau equation is studied in a parameter region in which the spatially homogeneous oscillations (corresponding to the limit cycle of the kinetics) are unstable, so that the dynamics are quite different from those of (1).

In all cases I will consider the solution that evolves from initial conditions of a small perturbation applied to the periodic plane wave solution with amplitude r_0. The results are independent of the details of the perturbation, and I will discuss the effects of using other initial conditions below. In all cases the equations are solved for a sufficiently long time that transients have decayed; details of this and other aspects of the numerical procedure are described in Appendix A. The cases $L = 5$ and $L = 30$ are chosen because they illustrate all of the solution types that I have observed in my more sporadic investigation of other points in the parameter space; however it may well be that there are quite different types of behaviour in other parameter regions. Most importantly, the results for $L = 30$ suggest an explanation for the phenomenon of irregular wakes behind invasive transition waves.

I begin by considering the relatively simple case of $L = 5$. The linear analysis discussed above predicts that in the unstable case, small perturbations to the periodic wavetrain will cause the solution to grow away from the wavetrain via spatiotemporal oscillations, with the form

$$r - r_0 \propto \mathrm{Re}\left[\rho(x)\exp(i\mathrm{Im}(\nu)t)\right], \tag{11a}$$

$$\theta - \lambda(r_0)^{1/2}x - \omega(r_0)t \propto \mathrm{Re}\left[\rho(x)\exp(i\mathrm{Im}(\nu)t)\right], \tag{11b}$$

where

$$\rho(x) = \sum_{i=1}^{4} k_i(\underline{v}_i)_1 \exp(\lambda_i x), \tag{11c}$$

$$\phi(x) = \sum_{i=1}^{4} k_i(\underline{v}_i)_3 \exp(\lambda_i x). \tag{11d}$$

As expected intuitively, as r_0 is decreased through $r_{0,crit}$ with $L = 5$, the solution of the full nonlinear equations (5) subject to (4) evolves to a solution that has the form (11), with an amplitude that tends to zero as the bifurcation point is approached. This is illustrated in Fig. 2, showing that the comparison with the linear solution (11) is extremely good.

As r_0 is decreased further with $L = 5$, the amplitude of the oscillations in the long term solutions for r and θ_x initially increases as expected, but then begins to decrease, at all points in space. Finally, at $r_0 \approx 0.45$, the long-term solution becomes a time invariant spatial pattern in r and θ_x, as illustrated in Fig. 3. As r_0 is decreased further, the pattern changes slightly, but the long term behaviour remains a stationary spatial pattern.

For larger values of L, the behaviour for r_0 just below $r_{0,crit}$ becomes very hard to determine, because the rate at which the amplitude of the r–θ_x oscillations increases with $(r_{0,crit} - r_0)$ becomes very rapid. This is

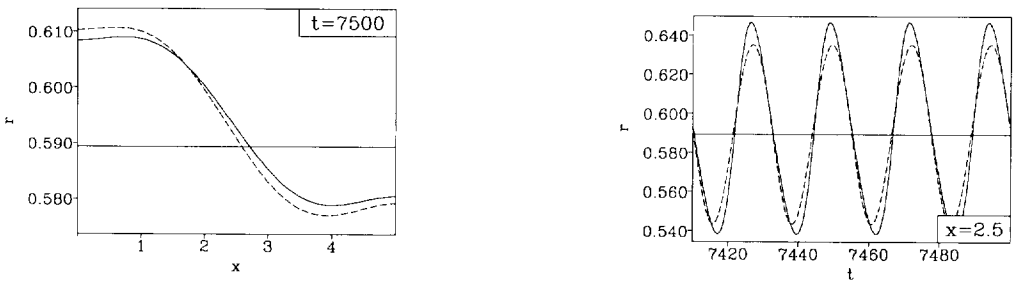

Fig. 2. The numerical solution (————) of (5) with (10) subject to (4) with $L = 5$ and $r_0 = 0.589$, which is just below $r_{0,crit} \approx 0.5894$, so that the periodic plane wave solution $r \equiv r_0$ is just unstable. The line $r = r_0$ is also drawn for comparison. The long term solution consists of regular spatiotemporal oscillations in r and θ_x (not shown, but of a qualitatively similar form). The numerical method is described in Appendix A. This partial differential equation solution is compared with the solution form (11) predicted by the linear analysis described in the text (- - - - - - - - -). The linear solution contains an arbitrary scaling in $(r - r_0)$ and also an arbitrary phase shift in time, and these are chosen to give the best agreement with the partial differential equation solution. The resulting linear solution compares extremely well with the numerical solution of the partial differential equations, and the comparison of the corresponding solutions for θ_x is equally good. Calculation of the linear solution requires determination of the eigenvalues and eigenvectors of the matrix $\underline{\underline{A}}$ (defined in the text) and also the constants $k_1, \ldots, k_4$, which are the elements of the left eigenvector of the matrix in (9); these eigenvalue and eigenvector calculations were all performed numerically. Note that all these vectors and matrices have complex entries.

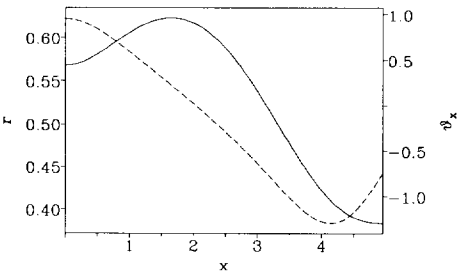

Fig. 3. The numerical solution for r (————) and θ_x (- - - - - - - - -) of (5) with (10) subject to (4) with $L = 5$ and $r_0 = 0.3$. The long term solution consists of a time invariant spatial pattern in r and θ_x. The numerical method is described in Appendix A.

Table 1
The variation with r_0 of the maximum and minimum of the long term temporal oscillations in r at $x = 0$ when the domain length $L = 19$

r_0	r_{max}	r_{min}	r_0	r_{max}	r_{min}
0.80050	0.8005	0.8005	0.79996	0.8303	0.7557
0.80030	0.8003	0.8003	0.79995	0.9180	0.1771
0.80010	0.8008	0.7994	0.79990	0.9181	0.0094
0.80000	0.8020	0.7981	0.79970	0.9175	0.0345
0.79997	0.8174	0.7789			

The periodic wavetrain $r \equiv r_0$ becomes unstable very close to the theoretically calculated bifurcation point $r_{0,crit}(19) \approx 0.8001$. The amplitude of the oscillations then increases extremely rapidly as r_0 is further reduced. In order to improve the precision of the calculated bifurcation value of r_0, a finer space mesh was used in these calculations than that described in Appendix A: 601 equally spaced mesh points were used. The numerical method was run up to a time $t = 20\,000$; again this is a longer time than that described in Appendix A to ensure that the final state has been reached (this requires a longer time close to the bifurcation point). Each pair of data points requires about 4 hours of computation on a Sun Sparcstation 20. The maximum and minimum of r are calculated over each mesh point after each time step during the interval $19\,000 \leq t \leq 20\,000$.

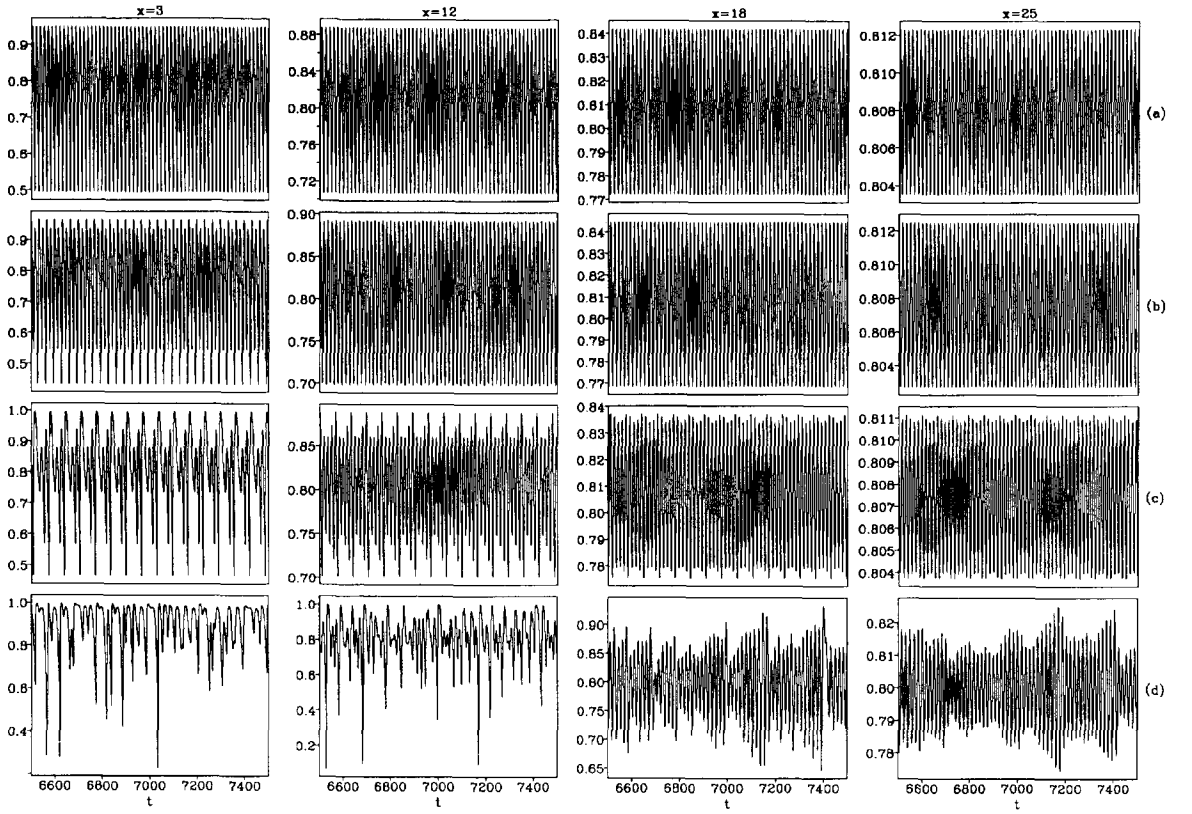

Fig. 4. The numerical solution for r of (5) with (10) subject to (4) with $L = 30$ and r_0 = (a) 0.808, (b) 0.8077, (c) 0.8075, (d) 0.8, (e) 0.54, (f) 0.48, (g) 0.415, (h) 0.2. The interpretation of these solutions is discussed in detail in the text. In each case the solution is plotted as a function of t at $x = 3$, 12, 18, and 25. The solution is recorded every 0.1 time units, so that each box contains 10000 data points joined by line segments. Note that detailed examination of the data points shows that a period doubling has occurred in the temporal behaviour between (a) $r_0 = 0.808$ and (b) $r_0 = 0.8077$ at all four values of x (and also at 20 other x values I have examined). However this is not visible in the plots at $x = 18$ and $x = 25$. The solutions for θ_x have qualitatively similar forms in all cases. The numerical method is described in Appendix A.

illustrated in Table 1 for $L = 19$, in which case the amplitude of the oscillations in r increases from zero (at $r_{0,crit}$) to about 0.7 (corresponding to large amplitude oscillations since r is constrained to lie between 0 and 1 [13]) during a change of 0.04% in r_0. In fact for $L = 30$, I have been unable to detect low amplitude oscillations in r. However for r just below $r_{0,crit} \approx 0.809$, the numerically calculated long term solution consists of simple temporal oscillations in r and θ_x at all points in space, albeit of large amplitude, as illustrated in Fig. 4a. As r_0 is decreased further, these temporal oscillations undergo period doubling at $r_0 \approx 0.8078$ (Fig. 4b); the period doubling appears to occur simultaneously at all points in space. At least two further period doublings then occur (Fig. 4c), again synchronously in space, until for $r_0 < 0.805$, the temporal oscillations appear irregular (Fig. 4d).

This irregular behaviour persists until $r_0 \approx 0.79$, when the oscillations become regular in what appears to be a sudden transition, and which occurs simultaneously at all space points. The period of the regular oscillations is approximately twice that of those occurring close to the instability curve and halves again at $r_0 \approx 0.77$, again synchronously in x.

As r_0 is decreased further, another transition towards irregular behaviour occurs, apparently via a bifurcation

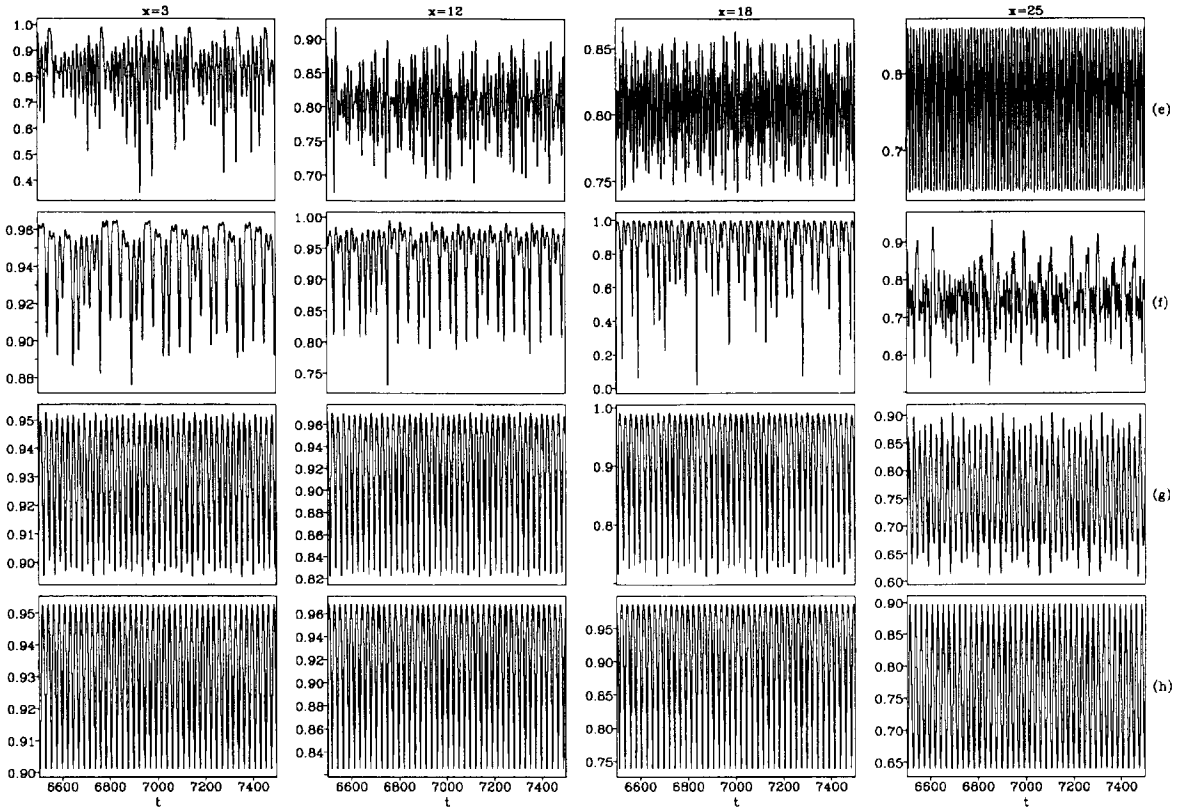

Fig. 4 — continued.

of the r–θ_x oscillations to a torus. In contrast to the period doubling described above, this does not occur simultaneously at all space points. Rather, it occurs initially at $x = 0$, and a 'wave of bifurcation' then moves across the domain in the positive x direction (Figs. 4e, 5a and 5b). Note that the polarity in the system is provided by the sign of θ_x imposed in the boundary condition; in the original u–v Eqs. (1), this corresponds to specifying the direction of motion of the periodic plane waves.

The temporal oscillations are irregular at all space points in the range $0.52 > r_0 > 0.45$ (Figs. 4f and 5c), and as r_0 is decreased from 0.45 to 0.4, the irregularity is lost, again through what appears to be a bifurcation via a torus to periodic oscillations. This reverse bifurcation sequence again occurs first at $x = 0$, and moves across the spatial domain in a 'wave of bifurcation' (Figs. 4g and 5d). For $r_0 < 0.4$, the long term behaviour is regular spatiotemporal oscillations in r and θ_x (Fig. 4h), and this persists down to $r_0 = 0$.

This complex sequence of long term behaviours is driven by the parameter r_0. However in the method of solution described above, r_0 affects both the initial and boundary conditions. In order to determine which of these was the key factor, I solved the equations with boundary conditions as above but with initial conditions given by a periodic plane wave of a different amplitude. In almost every case the long term behaviour is essentially the same for all amplitudes of the initial periodic plane wave, as well as for a variety of other initial conditions I have tried: the long term behaviour is determined purely by the value of r_0 in the boundary condition. The only exception I found to this was in the region of irregular behaviour around $r_0 = 0.5$, where two possible long term behaviours occur, depending on the initial wave amplitude (Fig. 6). One of these solutions is the irregular oscillations described above, while the other is consists of regular temporal oscillations at all space points: it appears that there are two attractors in the system in this parameter region, with rather

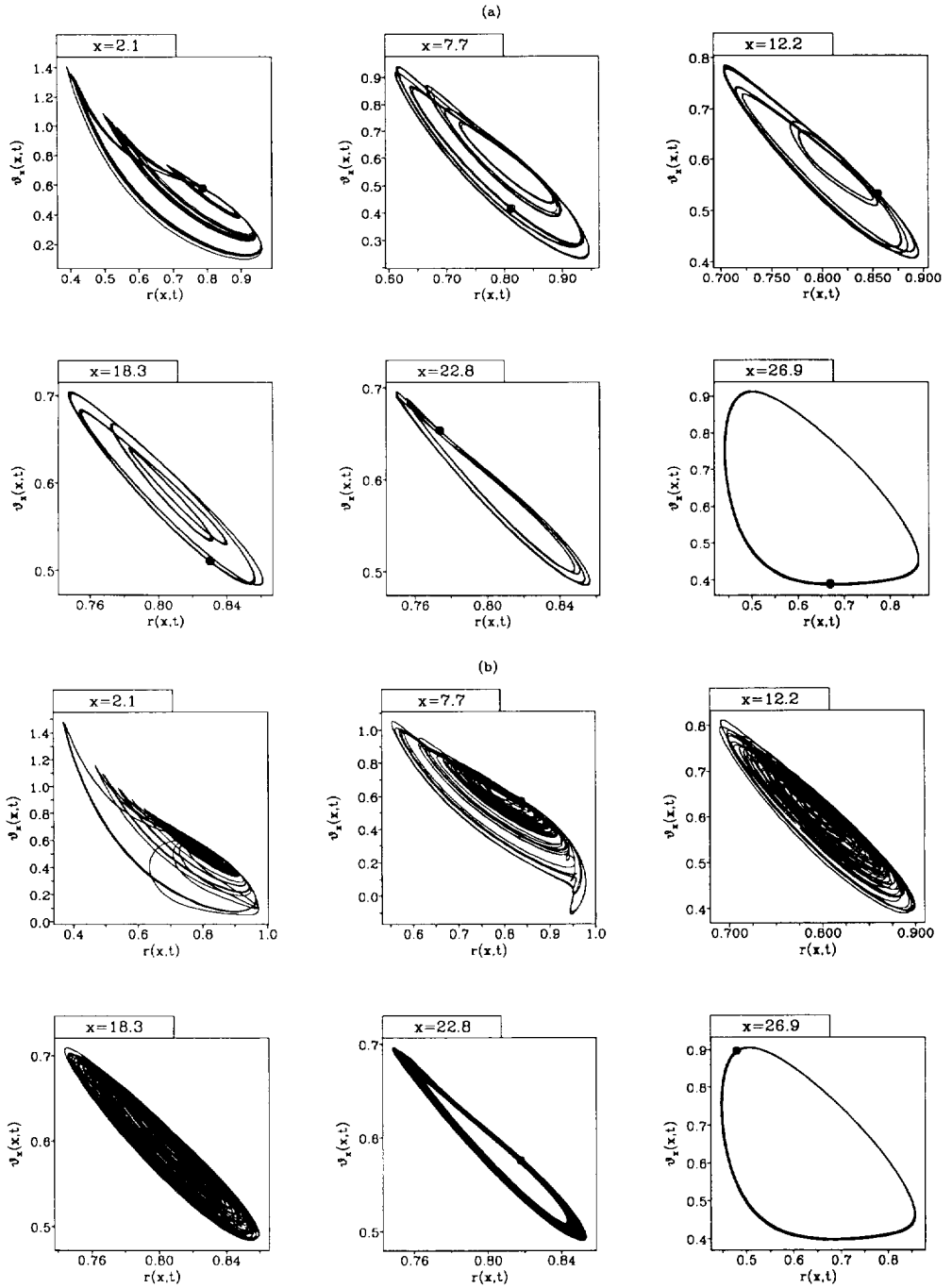

Fig. 5. The numerical solution of (5) with (10) subject to (4) with $L = 30$ and r_0 = (a) 0.5435, (b) 0.54, (c) 0.48, (d) 0.415. The solution is plotted in the r–θ_x plane at six different values of x; this method of illustratation shows the 'wave of bifurcation' described in the text. Each picture is obtained by connecting the values of r and θ_x every 0.1 time units for t in the interval $6500 \leq t \leq 7500$. On each r–θ_x plane a filled circle is superimposed (•), indicating the solution at $t = 6500$; however in some cases the mark is difficult to see. The numerical method is described in Appendix A.

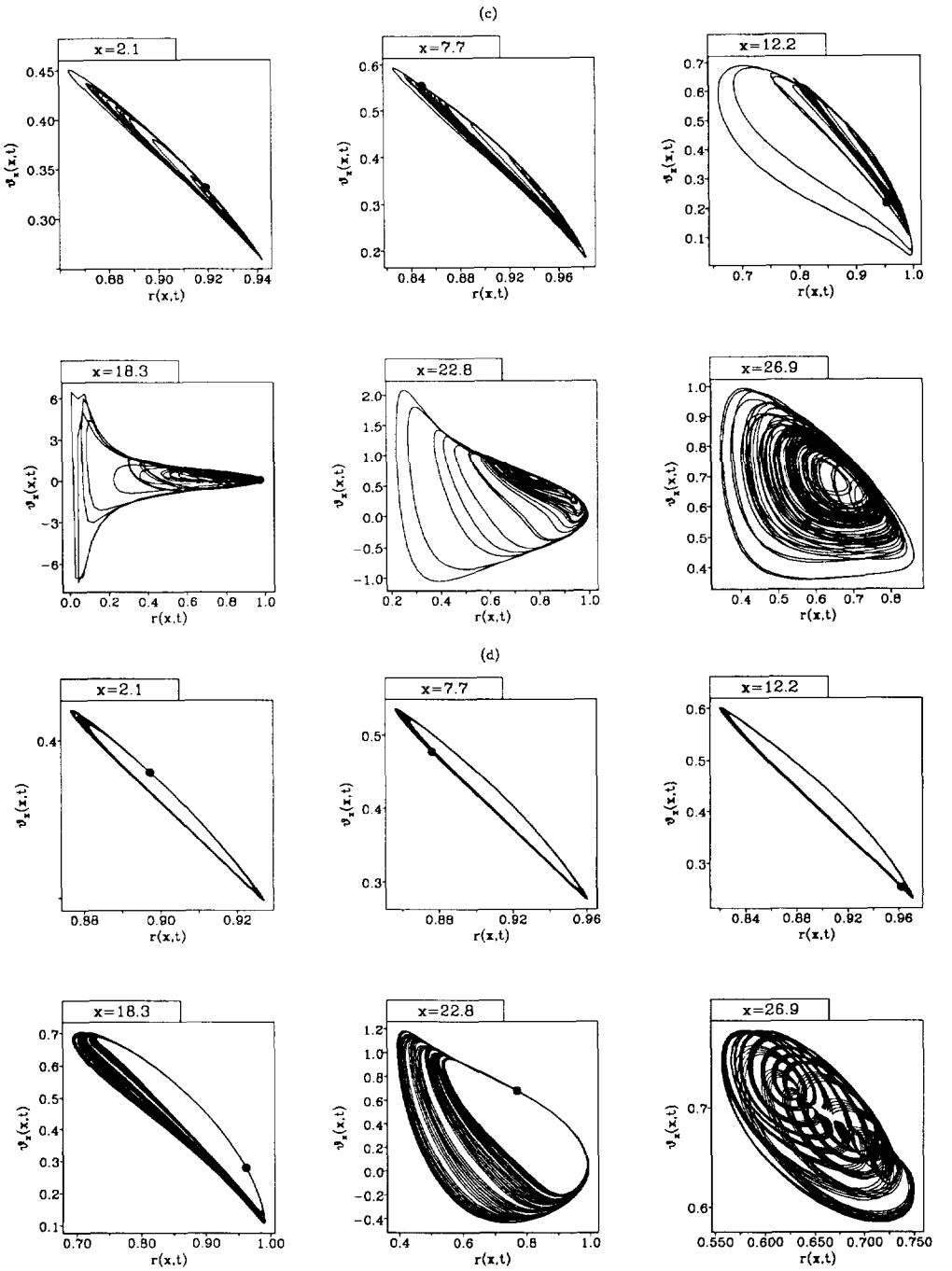

Fig. 5 — continued.

complex basins of attraction even for initial conditions restricted to periodic wavetrains (Fig. 6c).

Finally, it is also important to stress that the long term solutions I have described are very much boundary driven: if the boundary conditions are changed to zero flux ($u_x = v_x = 0$ at $x = 0$ and $x = L$) once the long term behaviour has been reached, the solution rapidly alters to spatially homogeneous oscillations, which are

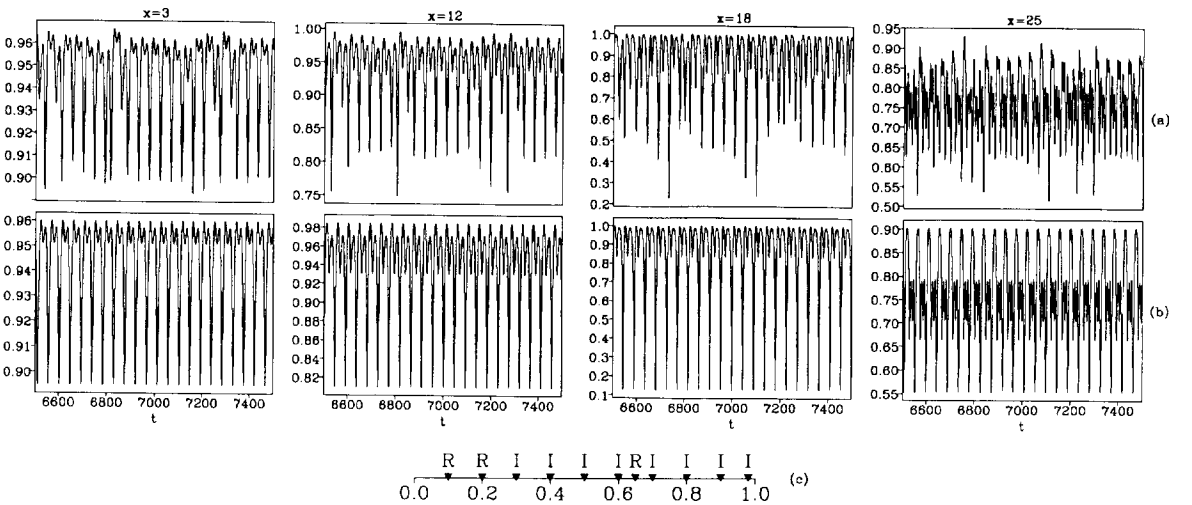

Fig. 6. (a),(b) The numerical solution of (5) with (10) subject to (4) with $L = 30$ and $r_0 = 0.5$, but with initial conditions given by a periodic plane wave of amplitude (a) 0.4 and (b) 0.65. These solutions illustrate the two different long term behaviours that I have observed for this value of r_0 in the boundary condition; which behaviour is obtained depends on the initial condition. In (c) I indicate the long term behaviour obtained for a series of initial wavetrain amplitudes: 'R' denotes regular oscillations (that is, the attractor illustrated in (b)) and 'I' denotes irregular oscillations (corresponding to (a)). This is in no sense a detailed description of the basins of attraction of the two long term behaviours – I have not attempted such a description. Rather, (c) simply illustrates that the final behaviour does depend sensitively on initial conditions for this value of r_0. I have only observed this sensitivity for values of r_0 close to 0.5: in all other cases the long term behaviour appears to be independent of initial conditions. In (a) and (b) I plot r as a function of t at four values of x; the solutions for θ_x are qualitatively similar. The numerical method is described in Appendix A.

just the limit cycle solution of the kinetics.

4. Application to irregular wakes

In previous publications, I have described the phenomenon of 'irregular wakes' behind invasive waves in reaction-diffusion equations [3,14]. The behaviour occurs in a number of directly applicable reaction-diffusion systems, including in particular ecological models for predator-prey interactions [4], but I will now summarise the phenomenon in the context of λ–ω systems, in which it is more simply described. The situation is a simple one; consider the system (1) in an infinite spatial domain, with $u = v = 0$ everywhere in space. Suppose now that a small perturbation is applied, locally in space, to this (unstable) steady state. The instability then propagates through the domain, away from the initial site of perturbation, leaving behind it a periodic wavetrain (Fig. 7a). This propagating wave corresponds to a transition wave front in r and θ_x, which are both constant in a periodic wavetrain. The amplitude of the wavetrain is uniquely determined, from the family of possible wave amplitudes, by the fact that the initial perturbation is spatially localised [14,15]. For the system (1) with $\lambda(.)$ and $\omega(.)$ given by (10), this amplitude is about 0.9 (see Appendix B), and condition (3) implies that the periodic wavetrain with this amplitude is stable. However if the form of $\omega(.)$ is changed, say to $\omega(r) = 3 - 3r^2$, then the amplitude becomes about 0.7, corresponding to an unstable wavetrain. Correspondingly, in this case the periodic plane waves behind the leading transition front destabilise, and one observes irregular spatiotemporal oscillations behind a band of regular period plane waves (Fig. 7b). This is the behaviour I have termed an "irregular wake".

A key question concerning such irregular wake regions is how the irregular behaviour arises from the dynamics

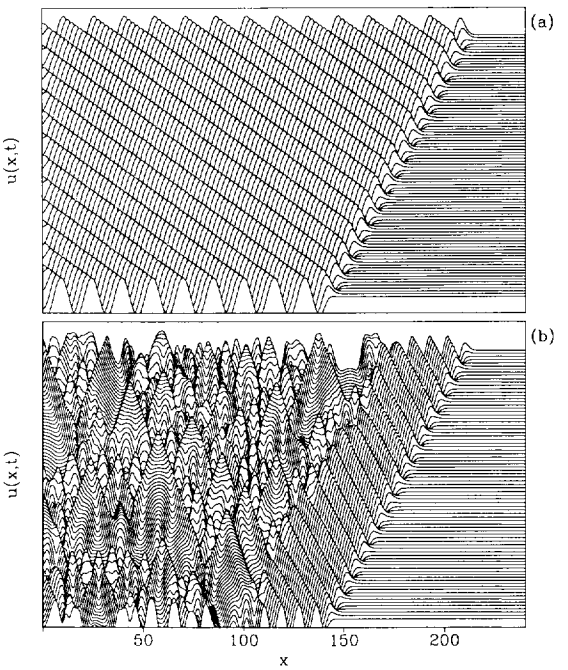

Fig. 7. Space–time plots of the numerical solution for $u(x,t)$ of (1) with $\lambda(r) = 1 - r^2$ and $\omega(r) = 3 - br^2$; (a) $b = 1$, (b) $b = 3$. The equation is solved on a large domain $0 \leq x \leq x_\infty$, subject to $u = v = 0$ at $x = x_\infty$ and with the symmetry condition $u_x = v_x = 0$ at $x = 0$. The boundary condition at $x = 0$ essentially plays no role [14] and simply enables the use of a semi-"infinite" rather than "infinite" domain, thus reducing the computer time required for solution. The domain length x_∞ is taken to be sufficiently large that further increase has a negligible effect on the solution over the time interval concerned. The numerical method is described in Appendix A, and a space mesh of 1001 equally spaced points was used, with $x_\infty = 250$. At $t = 0$, u and v were set to 0.1 at the first mesh point (on the $x = 0$ boundary), with $u = v = 0$ at the other mesh points; however, the solution is essentially the same for any initial perturbation that is localised in space [14]. In both (a) and (b) the solution is plotted as a function of x at successive times in the range $75 \leq t \leq 110$, with the vertical separation of solutions proportional to the time interval between them. The solution for v is qualitatively similar to that for u.

of the partial differential equations. This issue is particularly important because spatiotemporal irregularities are so rarely observed in reaction-diffusion equations, in sharp contrast to spatially discrete systems such as cellular automata and coupled map lattices, which often compete with reaction-diffusion equations as models of biological systems, and which frequently exhibit spatiotemporal chaos for realistic parameter values [16,17]. The results described above shed considerable light on this question. The transition wave front arising from the perturbation described above terminates at a particular periodic wavetrain, and thus one can conceptually regard the leading transition wave as imposing a boundary condition on the wake region of exactly the form $r_x = 0$, $\theta_x = \lambda(r_0)^{1/2}$. Of course the situation in the wake region is not the same as that discussed in the earlier part of the paper: in particular, the wake region continually grows in length and it has periodic plane waves of opposite direction of motion imposed at the two ends. However, notwithstanding these differences, the results presented above strongly suggest that the irregular behaviour observed in the wake region is driven by the forcing of a particular periodic wavetrain at its boundary.

Another important question concerning the irregular wakes is whether the behaviour is genuinely chaotic or whether it has underlying order despite its superficial irregularity. Again, the results described in the earlier part of the paper have important implications. The observation of period doubling and bifurcations to tori, which are well-known routes to chaos in finite dimensional dynamical systems, are strongly indicative that the irregular behaviour in the wake region is genuinely chaotic. Further evidence for this is given by exploring the

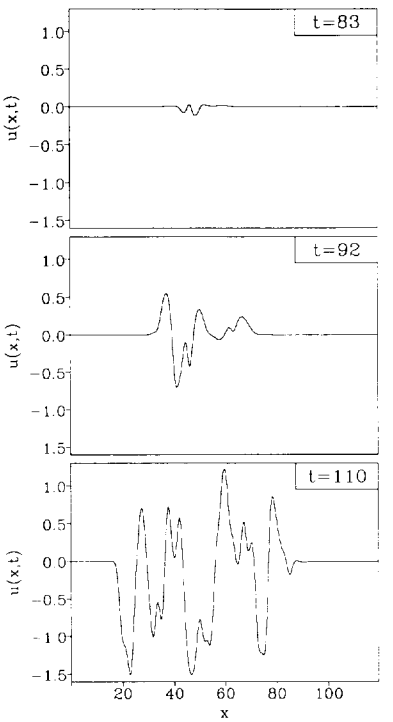

Fig. 8. The evolution of a small perturbation applied to the irregular wake region in the solution illustrated in Fig. 7b. The solution was solved up to a time $t = 75$ exactly as described in the caption to Fig. 7b, obtaining the solution at the first time illustrated there. I then continued the solution for two sets of initial conditions, one without any perturbation (simply the continuation of the numerical solution), and the other with a small perturbation applied to the middle of the irregular region: specifically 0.01 was added uniformly to u and v at all space points in the region $49 < x < 51$. The figure illustrates the development of this perturbation, calculated as the difference between the two solutions. The perturbation both grows and expands spatially as time increases. I plot only the difference in the u solutions; however the difference in the v solutions develops in a qualitatively similar way.

sensitivity of the wake region to perturbations. Specifically I have performed the following simple numerical test. I solve the system (1) for a sufficiently long time that an irregular wake has developed, such as in Fig. 7. I then continue the solution for two identical copies of the partial differential equation, in one case with a small perturbation applied locally at a point in the wake, and in the other without any perturbation. Calculating the difference between the two numerical solutions shows that the perturbation both grows and expands in time (Fig. 8). This demonstration of sensitivity to initial conditions, combined with the bifurcations described above, together constitute strong evidence that the behaviour behind the invading wave can properly be called a *chaotic* wake.

Appendix A

In this Appendix I describe briefly the details of the numerical method used to solve Eqs. (1). The basic method consists of the method of lines, which converts the partial differential equations to a set of coupled ordinary differential equations, which are then solved using Gear's method [18]. The solutions illustrated in Figs. 2 and 3 were obtained with a space mesh of 101 equally-spaced points, while those in Figs. 4 and 5 were obtained using 301 space points; the use of a finer mesh affects the precise values of r_0 at which the various

bifurcations occur, but has no affect on the basic forms of the long term behaviour that are observed. The time steps were controlled to obtain a solution accurate to at least 4 decimal places, and the equations were solved up to a maximum time of 7500. This is sufficiently long that further integration has a negligible effect on the form of the solution, at least for a trial set of r_0 values. The solution for one set of parameter values takes about 45 minutes on a Sun Sparcstation 20. Note that the r–θ equations (5) cannot be numerically solved directly because the variable θ increases without bound.

Appendix B

In this Appendix I derive an expression for the form of the periodic plane waves induced by a spatially localised perturbation to the state $u = v = 0$ in the system (1). The analysis is described in detail elsewhere [14], and here I present only a very brief summary. The leading wave front induced by the perturbation has the form of a transition wave of constant shape and speed in r and θ_x, with speed $2\lambda(0)^{1/2}$ [14]. Solutions of this type have the form $r = \hat{r}(z)$, $\theta = \hat{\theta}(z) + \omega(0)t$, where $z = x - 2\lambda(0)^{1/2}t$. Substituting these solution forms into (5) gives

$$\hat{r}'' + 2\lambda(0)^{1/2}\hat{r}' + \hat{r}\lambda(\hat{r}) - \hat{r}\hat{\theta}'^2 = 0,$$
$$\hat{\theta}'' + 2(\lambda(0)^{1/2} + \hat{r}'/\hat{r})\hat{\theta}' + \omega(\hat{r}) - \omega(0) = 0.$$

Non-trivial steady states of this system, that is with $\hat{r}$ and $\hat{\theta}'$ constant, satisfy

$$4\lambda(\hat{r})\lambda(0) = [\omega(\hat{r}) - \omega(0)]^2.$$

For the functional forms $\lambda(r) = 1 - r^2$, $\omega(r) = 1 - br^2$, this equation has a unique real solution:

$$\hat{r} = \left[\frac{2}{b^2}\left(\sqrt{1+b^2} - 1\right)\right]^{1/2},$$

while (3) implies that periodic plane waves are stable if and only if their amplitude is greater than $[2(1 + b^2)/(3 + 2b^2)]^{1/2}$. Comparing these, the waves in the wake region are stable if and only if b is less than the critical value $[(2\cosh\{(1/3)\cosh^{-1}(29/2)\} + 1)^2/9 - 1]^{1/2} \approx 1.15$.

Acknowledgements

This work was supported in part by grants from the Nuffield Foundation and the Royal Society of London. I am very grateful to Andrew Fowler (Oxford) and Mark Lewis (Utah) for helpful discussions.

References

[1] P.S. Hagan, SIAM J. Appl. Math. 42 (1982) 762.
[2] S. Koga, Prog. Theor. Phys. 67 (1982) 164.
[3] J.A. Sherratt, Physica D 70 (1994) 370.
[4] J.A. Sherratt, M.A. Lewis and A.C. Fowler, PNAS USA, submitted.
[5] H.G. Othmer, Lect. Math. Life Sci. 9 (1977) 57.
[6] D. Cope, SIAM J. Appl. Math. 38 (1980) 457.
[7] K. Maginu, J. Diff. Eqs. 31 (1979) 130.
[8] K. Maginu, J. Diff. Eqs. 39 (1981) 73.

[9] N. Kopell and L.N. Howard, Stud. Appl. Math. 52 (1973) 291.
[10] H.T. Moon, P. Huerre and L.G. Redekopp, Physica D 7 (1983) 135.
[11] L.R. Keefe, Stud. Appl. Math. 73 (1985) 91.
[12] L. Sirovich, J.D. Rodriguez and B. Knight, Physica D 43 (1990) 63.
[13] J.A. Sherratt, Nonlinearity 6 (1993) 1055.
[14] J.A. Sherratt, SIAM J. Appl. Math., in press.
[15] J.A. Sherratt, IMA J. Appl. Math. 52 (1994) 79.
[16] M.P. Hassell, H.N. Comins and R.M. May, Nature 353 (1991) 255.
[17] M.A. Nowak and R.M. May, Nature 359 (1993) 826.
[18] C.W. Gear, Numerical initial value problems in ordinary differential equations (Prentice-Hall, Englewood Cliffs, NJ, 1971).